CONFERENCE PRE-PRINT

PROGRESS ON NONLINEAR MHD MODELING OF FLUX PUMPING AND HYBRID SCENARIO FOR ASDEX UPGRADE PLASMAS

H. ZHANG[1,*], M. HOELZL[1], I. KREBS[2,3], A. BURCKHART[1], A. BOCK[1], S. GUENTER[1], V. IGOCHINE[1], K. LACKNER[1], R. RAMASAMY[1], H. ZOHM[1], JOREK TEAM[4], and ASDEX UPGRADE TEAM[5]

[1]Max Planck Institute for Plasma Physics, Garching, Germany
[2]Eindhoven University of Technology, Eindhoven, The Netherlands
[3]Dutch Institute for Fundamental Energy Research, Eindhoven, The Netherlands
[4]See author list of [M. Hoelzl et al 2024 Nucl. Fusion 64 112016]
[5]See author list of [H. Zohm et al 2024 Nucl. Fusion 64 112001]
[*]Email: haowei.zhang@ipp.mpg.de

Abstract

Flux pumping was achieved in recent hybrid scenario experiments in the ASDEX Upgrade (AUG) tokamak, which is characterized by a sawtooth-free helical quiescent state and the anomalous radial redistribution of toroidal current density and poloidal magnetic flux. The self-regulation mechanism of the AUG core plasma during flux pumping is investigated at realistic parameters using the JOREK code based on the two-temperature, nonlinear, full magnetohydrodynamic (MHD) model. A key milestone in AUG flux pumping modeling is achieved by quantitatively reproducing the clamped current density and safety factor profiles in the plasma core, demonstrating the effectiveness of the dynamo effect in sustaining the flux pumping state. The dynamo term, of particular interest, is primarily generated by the pressure-gradient driven 1/1 quasi-interchange-like MHD instability. The work systematically extrapolates the parameter regimes of flux pumping from the above AUG base case by scanning dissipation coefficients and plasma beta. The simulation results reveal bifurcated plasma behaviour, including distinct states such as flux pumping (helical core with a flat current density), sawteeth (periodic kink-cycling), single crash (without subsequent cycle), and quasi-stationary magnetic island (peaked current density). The relationships between system dissipation, plasma beta, and different plasma states are carefully analyzed. The modeling efforts advance the understanding of flux pumping and facilitate the development of a fast surrogate model for efficient evaluation of flux pumping.

1. INTRODUCTION

Sawtooth control is essential for long-pulse operations in next-generation tokamaks like ITER and DEMO [1]. To address this need, the self-regulating flux pumping mainly achieved in the hybrid scenario offers a potentially robust solution [2–7]. Experimentally, flux pumping is identified by the anomalous radial redistribution of central current density (equivalent to poloidal magnetic flux) during the quiescent sawtooth-free phase with m/n = 1/1 instability (m and n are the poloidal and toroidal mode numbers, respectively) [3–7]. The redistribution clamps the on-axis safety factor (q_0) near unity and prevents sawtooth onset. Theoretically, flux pumping has been carefully studied through qualitative nonlinear magnetohydrodynamic (MHD) modeling. Such efforts reveal the critical role of dynamo effect, predict the positive correlation between the efficiency of flux pumping dynamo and the poloidal plasma beta (β_p) [8, 9], and assess the role of bootstrap current in flux pumping in the low-density regime [10]. Recent JOREK simulations enable a quantitative comparison between MHD modeling and AUG experiments, showing consistent current density deficit and dynamo electric field during flux pumping [11], and establishing the foundation for the next stage of modeling of JET flux pumping experiments [5, 7].

In retrospect, nonlinear MHD modeling has proven to be crucial for assessing the operating window of flux pumping in tokamaks. In the 1980s, the 1/1 convection cell driven by resistivity (η)/temperature gradient was modeled with a reduced MHD model [12], where the sawtooth-free solution is more readily obtained at low heat conductivities (χ) and at larger ratios of resistive time to Ohmic-heating time. In

the 2010s, different regimes of stationary helicity and sustained kink cycles were investigated with the $\eta\chi$MHD model in the XTOR-2F code [13], showing a threshold in β_p for the stationary solution, with a lower $\chi_\perp$ favoring the kink cycling. A subsequent work of XTOR-2F, incorporating the two-fluid effect, studying the diamagnetic threshold for sawtooth cycling [14] found that the stationary helical state prefers regimes with weak ion-diamagnetic drift and high resistivity. Recently, the problem was further studied by other codes based on visco-resistive full MHD model. The small sawtooth or the steady state with 1/1 magnetic island was obtained in both high- [15] and low-viscosity [16] regimes. The plasma beta threshold for flux pumping was confirmed in [16], consistent with [9, 13].

In addition to tokamak plasmas, self-organized states — namely the single-helicity (SH) and quasi single-helicity (QSH) states — have also been a major research focus for reversed field pinches (RFPs). The SH/QSH states are distinct from the more common multiple helicity (MH) state, which is manifested by periodic sawtooth-like relaxations and a wide spectrum of MHD modes due to magnetic reconnections [17,18]. Through MHD modeling of the RFX-mod device, different plasma regimes of SH/QSH and MH states were identified and compared with experiments. A key finding is that the SH/QSH state predominates under two distinct conditions: (i) low Hartmann numbers (high system dissipation) with ideal boundary conditions [17, 18]; or (ii) high Hartmann numbers (low system dissipation, more consistent with experiments) with a helical boundary condition [19, 20]. The relevant dynamo effect responsible for sustaining the SH/QSH state in RFP was analyzed [18] and extrapolated to tokamak [21], yielding a similar profile of dynamo electric field in the laminar helical states of both device types.

The outlined research substantially improved the understanding of self-regulating plasma dynamics and current density redistribution mechanism during flux pumping. However, the approximate flux pumping parameter space remains undetermined, particularly in the low-dissipation regime that is more relevant to experiments. The uncertainty complicates the experimental search for flux pumping on existing devices and complicates the scenario design for future ones. Based on the achieved quantitative modeling of flux pumping for AUG discharge [11], the main objective of this work is to investigate the parameter regimes of flux pumping in AUG within the single-fluid framework, with a particular focus on viscosity, resistivity and plasma beta. 3D nonlinear modeling predicts the bifurcation of core plasma dynamics into different states, including quasi-stationary flux pumping, sawteeth (kink cycling), etc. The findings are generally consistent with existing literature, and they offer insights into the core plasma physics at conditions much closer experiments. Nevertheless, there is still a noticeable difference in the plasma beta threshold for flux pumping between the single-fluid MHD modeling and AUG experiments, highlighting the need for the ongoing extended modeling including the two-fluid effect [14] and kinetic energetic particle (EP) physics (e.g., fishbones) [3, 22, 23] to more precisely predict the operating window of flux pumping.

2. AUG FLUX PUMPING DISCHARGE AND 3D MHD MODELING

Reproducible phases of flux pumping and sawteeth were obtained in AUG discharge #36663 by adjusting the NBI (Neutral Beam Injection) heating power and the co-ECCD (Electron Cyclotron Current Drive) intensity [3]. The sawtooth-free flux pumping state was specifically obtained at high normalized plasma beta ($\beta_N \sim 3$) and a moderate ECCD (~ 0.10MA), in contrast to the two sawtoothing phases obtained at either lower β_N (~ 2) or higher ECCD (~ 0.15MA), see Fig. 3 of [3]. The deficits in the central current density ($\delta J_\varphi \simeq -2\text{MA/m}^2$) and toroidal electric field ($\delta E_\varphi \simeq -8\text{mV/m}$) were identified by comparing the IDE (integrated data analysis equilibrium) solutions with and without considering the flux pumping mechanism (by including or excluding the Imaging Motional Stark Effect (IMSE) diagnostic data in IDE reconstructions), as shown by Fig. 4 of [3]. The experimental analyses demonstrate an anomalous radial redistribution of current density in the presence of 1/1 mode during the flux pumping phase.

To understand the self-regulating plasma dynamics during flux pumping, 3D quantitative nonlinear full MHD simulations have been carried out at realistic parameters of the flux pumping phase of AUG discharge #36663 ($q_0 \simeq 1.0$, $\beta_N \simeq 3.0$, plasma current $I_p \simeq 0.80$MA, $\eta \sim 10^{-9}\Omega\cdot$m, kinematic viscosity $\mu \sim 3\text{m}^2/\text{s}$) [3,11]. Compared with the published results of [11], minor improvements have been made to the simulation below by (i)

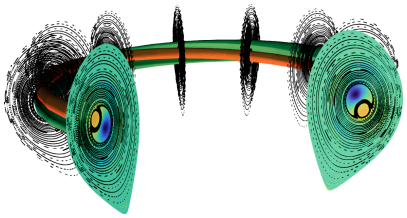

FIG. 1. The quasi-stationary magnetic flux tubes in the 3D simulation of the AUG flux pumping discharge. The colored slices indicate the mode structure of toroidal magnetic field.

introducing the equipartition terms in the temperature equations of ions and electrons for a more precise depiction of temperature and resistivity; (ii) applying isotropic resistivity in the Ohm's law with appropriate current sources instead of only in the toroidal direction. The 3D simulation presents a quasi-stationary helicity with two twisted flux tubes, as shown by Fig. 1. The 1/1 mode dominates the 3D simulation across a resistive timescale of seconds, which is consistent with the experiments [3].

A comparative analysis shown in Fig. 2 was conducted between the 3D flux pumping modeling and the 2D modeling. The 2D case excludes MHD instabilities and focuses on the effect of the non-inductive current source in the 2D equilibrium evolution. The non-inductive current source equals to the sum of NBI, ECCD, and bootstrap current, as shown in Fig. 19 (a) of [11]. The saturated q profile over the radial coordinate ρ_p $(= \sqrt{\psi_n})$ from the 2D simulation is plotted by the solid line in Fig. 2 (a), where q_0 decreases to 0.6. A value of $q_0 \ll 1$ is typically indicative of internal kink mode and sawtooth onset, which contradicts the experimental observation (sawtooth-free). In contrast, the 3D simulation with a dominant 1/1 mode shows that the saturated q_0 remains close to unity in the core, see the dashed line in Fig. 2 (a). The comparison of toroidal current density in Fig. 2 (b) confirms the discrepancy in q profiles. In the 2D simulation, the central current density undergoes an increase from 2.4 MA/m^2 to 4 MA/m^2. However, in the 3D simulation, it is clamped around 2.5 MA/m^2, suggesting an effective redistribution of current density by the 1/1 mode induced flux pumping.

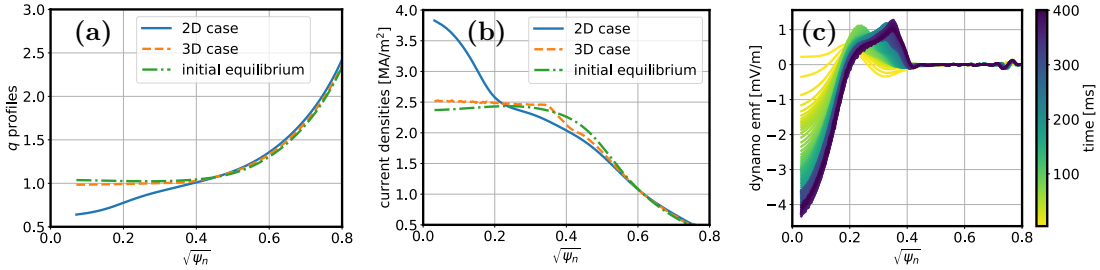

FIG. 2. (a) q and (b) current density profiles at the saturated stages of the 2D (solid line) and 3D (dashed line) simulations, as well as of the initial equilibrium (dash-dotted line). (c) The parallel dynamo electric field vs. time from the 3D simulation.

The current redistribution mainly results from the MHD dynamo generated by the 1/1 MHD instability [8], which exhibits characteristics of both quasi-interchange and tearing mode in the AUG modeling [11]. As shown in Fig. 2 (c), the dynamo electric field along the axisymmetric magnetic field ($\mathbf{b}_0$) is mainly generated by n = 1 non-axisymmetric components of plasma velocity $\tilde{\mathbf{v}}$ and magnetic field $\tilde{\mathbf{B}}$, i.e., $\varepsilon_\parallel = \langle(\tilde{\mathbf{v}} \times \tilde{\mathbf{B}}) \cdot \mathbf{b}_0\rangle$, where $\langle \cdots \rangle$ denotes flux surface average. The dynamo generates a negative toroidal loop voltage of the order of mV/m in the core ($\rho_p < 0.2$), which equivalently increases the current diffusion. In the region beyond the plasma core ($0.2 < \rho_p < 0.4$), the dynamo loop voltage is positive, thereby increasing the current density. The reverse distribution of dynamo loop voltage continuously redistributes the current density and magnetic flux from the core region outward. As a result, the current density profile maintains a flat profile across a substantial radius ($\rho_p < 0.4$), and q_0 remains close to unity. The saturated q profile, current density, and the dynamo electric field from the 3D simulation agree well with the experimental profiles reconstructed by including IMSE data during the flux pumping phase, as shown by Fig. 3 (reprinted from [3]).

Compared with previous MHD modeling with lower Hartmann numbers $10^3 \lesssim H \lesssim 10^6$ [9, 15–21], the presented quantitative MHD modeling of flux pumping at experimental parameters demonstrates that the sawtooth-free quasi-stationary solution is also accessible at extremely low system dissipations (the Hartmann number $H \simeq 10^8$, the magnetic Prandtl number $P \simeq 1.4 \times 10^3$, the Lundquist number $S \simeq 3 \times 10^9$, and the viscous Lundquist number $S_\mu \simeq 2 \times 10^6$). On this basis, the subsequent section systematically investigates the parameter regimes for bifurcations towards different plasma states, typically represented by flux pumping and sawteeth.

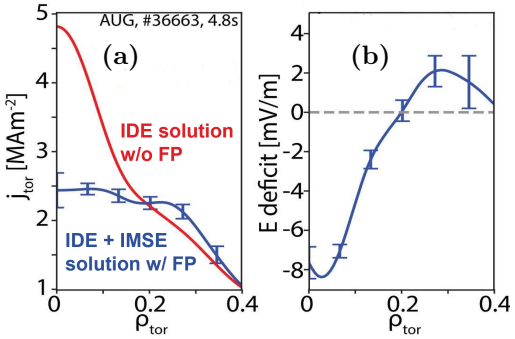

FIG. 3. Reconstructed profiles of the flux pumping phase at 4.8s of the AUG discharge #36663: (a) experimental (blue, with IMSE data) and modeled (red, without IMSE data) current densities; (b) corresponding effective electric field deficit. Reprinted from [3].

3. FLUX PUMPING AND BIFURCATIONS AT DIFFERENT PARAMETERS

The full MHD equations used in this study are available in [11]. To facilitate the discussion, three characteristic times are defined: the resistive diffusion time $\tau_R = \mu_0 L^2/\eta$, the viscous time $\tau_\mu = L^2/\mu$, and the Alfvén time $\tau_A = L/v_A$, where μ_0 the vacuum magnetic permeability, L the characteristic spatial scale, η the resistivity, μ the kinematic viscosity, $v_A = B_0/\sqrt{\mu_0\rho_0}$ the Alfvén velocity, B_0 and ρ_0 the on-axis magnetic field strength and mass density. Following similar normalization procedure as [18]: $t' = t\sqrt{\tau_\mu/\tau_R}/\tau_A$, $\mathbf{v}' = \mathbf{v}\sqrt{\tau_R/\tau_\mu}/v_A$, $\rho' = \rho/\rho_0$, $\nabla' = L\nabla$, $\mathbf{B}' = \mathbf{B}/B_0$, $p' = \mu_0 p/B_0^2$, $\mathbf{J}' = \mu_0 \mathbf{J} L/B_0$, $\mathbf{S}_j' = \mu_0 \mathbf{S}_j L/B_0$, the induction equation and momentum equation can be rewritten as (ignore $'$ for normalized quantities)

$$\frac{\partial \mathbf{B}}{\partial t} = \nabla \times (\mathbf{v} \times \mathbf{B}) - \nabla \times \left[H^{-1} (\nabla \times \mathbf{B} - \mathbf{S}_j)\right], \tag{1}$$

$$P^{-1}\left(\frac{\partial \mathbf{v}}{\partial t} + \mathbf{v}\cdot\nabla\mathbf{v}\right) = \frac{1}{\rho}\left[(\nabla\times\mathbf{B})\times\mathbf{B} - \nabla p + \nabla\cdot\left(H^{-1}\nabla\mathbf{v}\right)\right]. \tag{2}$$

It is found that beyond the equilibria and source terms, the nonlinear MHD system is mainly governed by two dimensionless parameters H and P [17, 18], where the Hartmann number $H \equiv \sqrt{\tau_R\tau_\mu}/\tau_A = \sqrt{\mu_0/(\eta\mu)}Lv_A$, and the magnetic Prandtl number $P \equiv \tau_R/\tau_\mu = \mu_0\mu/\eta$. For specific cases with ignorable inertia terms on the left-hand side, H is the unique control parameter for the plasma state, which is inversely proportional to the system dissipation. The adopted model exhibits slight discrepancies from the prior dual-field MHD model (only solving for $\mathbf{v}$ and $\mathbf{B}$) in RFP modeling [17, 18]: (i) the pressure gradient enters the system and introduces an additional degree of freedom in the driving intensity for the mode; (ii) the density is not fixed although it is expected to be stable in nonlinear 3D simulations.

First, to evaluate the influence of the overall system dissipation (represented by the Hartmann number) on the core plasma state, the ratio of μ/η is fixed same as the base case ($\eta_{\rm base} = 2.41 \times 10^{-9}\Omega$m, $\mu_{\rm base} = 2.7{\rm m}^2/{\rm s}$, $P = 1400$) in Sec. 2. Then, μ and η are increased simultaneously to decrease H. Four representative cases are simulated respectively at the increased η and μ by (a) $10\times$, (b) $10^2\times$, (c) $10^3\times$, and (d) $10^4\times$, corresponding to decreasing H by (a) $10^{-1}\times$, (b) $10^{-2}\times$, (c) $10^{-3}\times$, and (d) $10^{-4}\times$. Four different plasma states are obtained at varying dissipation levels, as shown by the temporal evolutions of q_0 in Fig. 4. For the two low dissipation cases [the base case and case (a), $H = 7.9\times10^7$ and $\times10^6$], the quasi-stationary flux pumping solution is obtained and q_0 remains close to unity throughout. However, as the dissipation is further increased by one order of magnitude [case (b), $H = 7.9\times10^5$], the plasma core exhibits the sawtooth-like kink cycling state with q_0 oscillating between 0.93 and 1.0. The oscillations of pressure and current density on the axis are also observed (not shown). Furthermore, when the dissipation is increased to reach $H = 7.9\times10^4$ in case (c), q_0 first decreases below 0.7 and then triggers a giant sawtooth crash (q_0 recovers to unity quickly). Afterwards, q_0 saturates at approximately 0.92 for hundreds of normalized time units until the simulation terminates at $t = 1000$. The late stage is analogous to the saturated 1/1 resistive internal kink mode. For the last case (d) with the highest dissipation and $H = 7.9\times10^3$, q_0 decreases dramatically in a short timescale smaller than 100 and then saturates around 0.7 for thousands of normalized time units. The q_0 evolution of case (d) is similar to the 2D case, though a 1/1 magnetic island is observed in the plasma core, suggesting that the 1/1 mode may not affect the q profile here. The aforementioned cases are categorized into four types based on the distinct characteristics of q_0 evolution: (i) the flux pumping state (FP), (ii) the sawtooth state (ST), (iii) the single-crash state (SC) followed by a quasi-stationary 1/1 magnetic island, and (iv) the quasi-stationary 1/1 magnetic island state (QS), respectively.

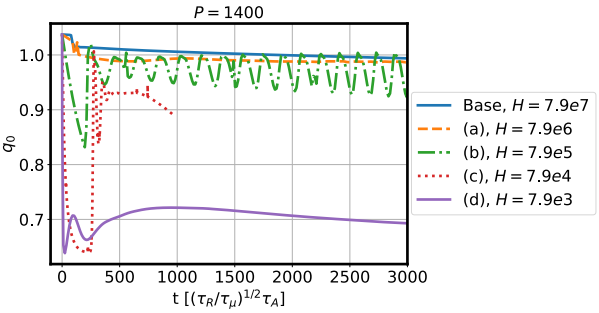

FIG. 4. Different plasma states obtained at different system dissipations: Base case with $H = 7.9\times10^7$ (blue solid line); case (a) with $H = 7.9\times10^6$ (orange dashed line); case (b) with $H = 7.9\times10^5$ (green dash-dotted line); case (c) with $H = 7.9\times10^4$ (red dotted line); and case (d) with $H = 7.9\times10^3$ (purple solid line). P is fixed at 1400 for all cases.

The temporal evolutions of the dynamo electric field (normalized by the increased ratio of resistivity) for cases (a-d) are plotted in Fig. 5. In all three cases (a-c) with prominent dynamo activities, the dynamo profile is similar to Fig. 2 (c). In the flux pumping case (a) shown by Fig. 5 (a), the dynamo

remains stable around the normalized amplitude of $0.004 \sim 0.007$ after $t = 1000$, although a limited slow oscillation is observed after $t = 2000$. The stable dynamo is responsible for maintaining the saturated $q_0 \simeq 1.0$ in the flux pumping case by redistributing the applied non-inductive current source. In contrast, the dynamo in the sawtoothing case (b) oscillates at the same frequency as q_0, as shown by Fig. 5 (b). The maximum normalized dynamo amplitude during the sustained sawtooth cycles is about 0.007, which flattens the current density on a timescale much shorter than the resistive diffusion, thereby appearing mainly at the rising phase of q_0. After the 1/1 magnetic island replaces the original magnetic axis and restores the axisymmetric flux surfaces, the dynamo amplitude decreases to a negligible magnitude due to the decay of the pumping 1/1 resistive internal kink mode. For case (c) with the single crash in Fig. 5 (c), a strong dynamo of the normalized magnitude of 0.012 is observed at $t = 270$, lifting q_0 from 0.65 to unity on a short timescale of $\sim 20(\tau_R/\tau_\mu)^{1/2}\tau_A$ (~ 0.34 ms). Afterwards, the normalized amplitude of dynamo saturates around 0.003 and maintains q_0 around 0.9 without further crashes. For case (d) with a quasi-stationary 1/1 magnetic island as depicted in Fig. 5 (d), the normalized dynamo amplitude is at the noise level and not able to counteract the current source anymore. Therefore, the temporal evolution of q profile resembles the 2D case with $q_0 \ll 1.0$.

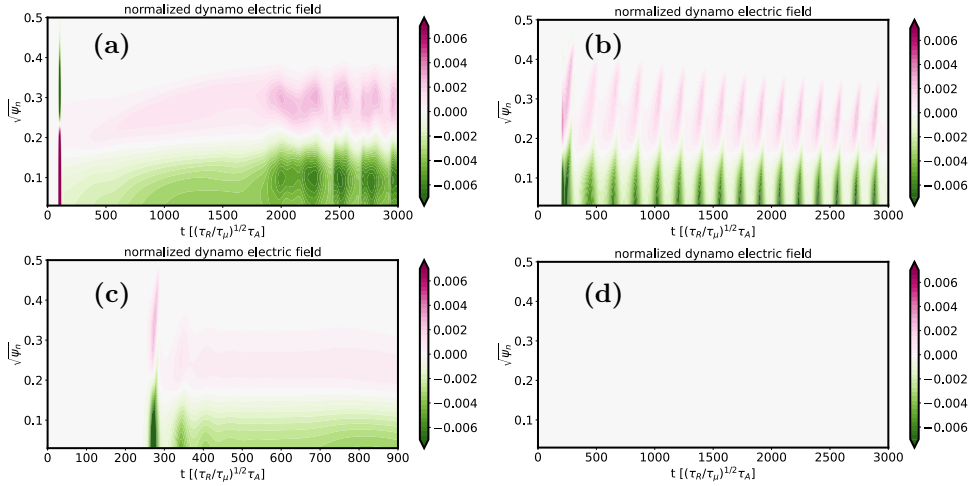

FIG. 5. Temporal evolutions of the radial profile of dynamo electric field normalized by the increased ratio of resistivity, respectively for cases (a) $10 \times \eta_{\rm base}$, (b) $10^2 \times \eta_{\rm base}$, (c) $10^3 \times \eta_{\rm base}$, and (d) $10^4 \times \eta_{\rm base}$. P is fixed at 1400 for all cases.

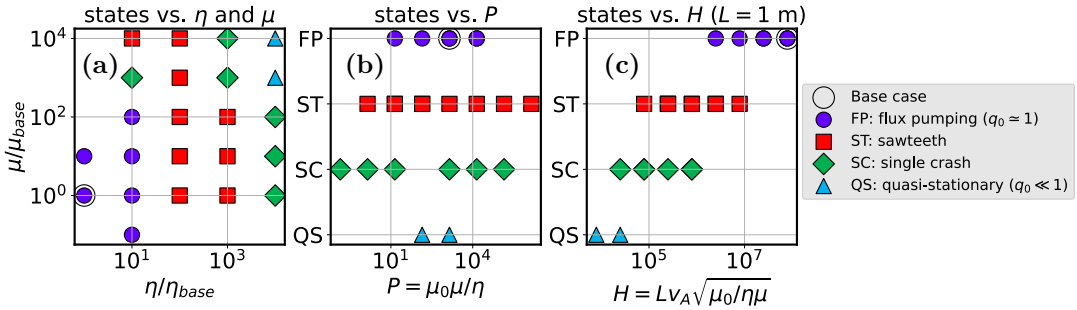

FIG. 6. Different plasma states obtained by scanning viscosity and resistivity over a broad 2D parameter space from $1 \times \eta_{\rm base}$ to $10^4 \times \eta_{\rm base}$ and from $0.1 \times \mu_{\rm base}$ to $10^4 \times \mu_{\rm base}$ (a). The dependencies of plasma states are plotted against the magnetic Prandtl number (b) and the Hartmann number (c).

The viscosity and resistivity of interest are further extrapolated to a broad 2D map from $1 \times \eta_{\rm base}$ to $10^4 \times \eta_{\rm base}$ and from $0.1 \times \mu_{\rm base}$ to $10^4 \times \mu_{\rm base}$. The plasma state for each set of viscosity and resistivity is illustrated in Fig. 6 (a). The diagram shows that flux pumping can be obtained at relatively low dissipation, as shown by the cycles in the lower left corner of Fig. 6 (a). Conversely, the sawtooth and single-crash states with sawtooth relaxation are obtained at moderate dissipation (rectangles and diamonds). The quasi-stationary island state is only accessible at extremely high dissipation (up triangles). Meanwhile, there is an absence of clear dependence of plasma states on the magnetic Prandtl number in this tokamak modeling, as evidenced by Fig. 6 (b), which is qualitatively consistent with the RFP modeling [17, 18]. Instead, the transitions of plasma states can be more intuitively represented by the Hartmann number, which acts as a reverse proxy for system dissipation. As shown by Fig. 6 (c),

from low Hartmann number $H \sim 10^3$ to high Hartmann number $H \sim 10^8$, the plasma state transits from quasi-stationary island, single-crash state, sawtooth, and flux pumping in sequence. The strong dependency of central plasma states on the Hartmann number resembles the RFP modeling. Though in the early modeling of RFX-mod, the laminar QS/QSH state is obtained at low Hartmann number ($H \lesssim 10^3$) [17, 18]. In the recent modeling with helical boundary conditions, the QS/QSH state is also reproduced at experimentally relevant regimes ($H \gtrsim 10^5$) [19, 20].

The amplitudes of the normalized dynamo electric field for all cases in Fig. 6 are plotted in Fig. 7 over the increased ratio in resistivity for each viscosity. Note that the dynamo amplitude is represented by the maximum value during the sustained sawtooth oscillations or the stable value after the first crash for the single-crash case. The normalized amplitude of the dynamo electric field indicates the capability of the 1/1 mode to counteract the current drive such that q_0 can be continuously sustained at or periodically recovered to unity, either through flux pumping or sawtooth relaxation. For the cases with relatively low viscosities ($\mu/\mu_{\rm base} \leq 10^2$), the normalized dynamo remains roughly stable as the resistivity increases, with a weak scaling of $\propto \eta^{0.11}$. For most cases, the dynamo term is comparable to the intensity of current drive, thereby maintaining q_0 much larger than that of the 2D case ($q_0 \sim 0.6$). Nevertheless, there are two distinct points in Fig. 7 at $\eta/\eta_{\rm base} = 10^4$, where the dynamo amplitude dramatically falls below the average ($\sim 10^{-3}$). These two cases correspond to the quasi-stationary island state in Figs. 4-6. The absence of dynamo electric field results in the peaking of central current density and the drop in q_0, which are more analogous to the 2D situation.

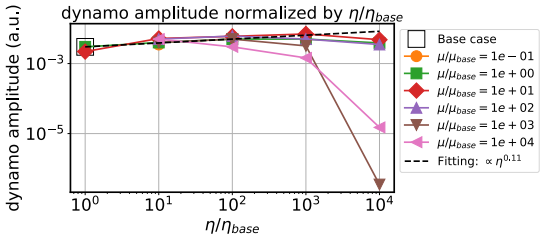

FIG. 7. The amplitudes of the dynamo electric field normalized by the increased ratio of resistivity for call scanned cases from $1\times\eta_{\rm base}$ to $10^4\times\eta_{\rm base}$ and from $0.1\times\mu_{\rm base}$ to $10^4\times\mu_{\rm base}$.

3D nonlinear MHD modeling of flux pumping remains computationally time-consuming. The surrogate model being developed aims to predict the accessibility of flux pumping efficiently with a flight simulator [24]. Prior to this, the underlying relationship between the linear growth rate of the 1/1 (resistive) quasi-interchange mode of the 3D simulations and the current peaking timescale of the 2D simulations is investigated. The growth rate and current peaking timescales are normalized following the same procedure for Eqs. 1 and 2. As shown in Fig. 8, flux pumping is mainly accessible when the normalized linear growth rate of the mode is sufficiently large ($\gtrsim 10^{-1}$) and the normalized characteristic current peaking timescale is long enough ($\gtrsim 10^4$). Otherwise, states with sawtooth relaxations are likely to be retained. The primary benefits of bridging plasma states with the linear growth rate and current peaking timescale are largely attributed to the reduced requirement of computational resources, as only the 2D modeling and linear phase of 3D cases are needed. The larger growth rate potentially indicates a stronger nonlinear dynamo term generated by the instability, and the longer current peaking timescale corresponds to a lower current driving efficiency, thereby favoring the flux pumping. Nevertheless, more in-depth analyses are necessary to build the knowledge to accurately assess the feasibility of flux pumping without full-cycle 3D nonlinear MHD modeling.

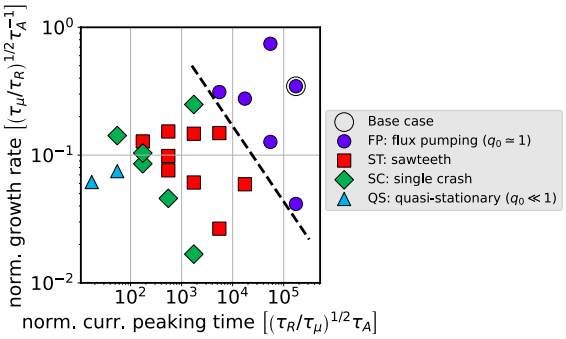

FIG. 8. The plasma states classified by the linear growth rate of 1/1 (resistive) quasi-interchange mode in 3D simulations and the current peaking times in 2D simulations. The growth rate and current peaking time are normalized with the same method as Eqs. 1 and 2. The dashed line roughly marks the boundary for accessing flux pumping.

This paper further investigates the dependence of plasma states on plasma beta (β_N and β_p, the latter is evaluated at half the minor radius). The q profile of the initial equilibria and the current source term remain the same as the base case. However, the pressure and heating sources are scaled down synchronously to obtain equilibria with lower β. 3D simulations at different β and Hartmann numbers (the magnetic Prandtl number is fixed at 1400) yields different plasma states as shown by Fig. 9, including flux pumping, sawteeth, and the transition between flux pumping and sawteeth, etc.

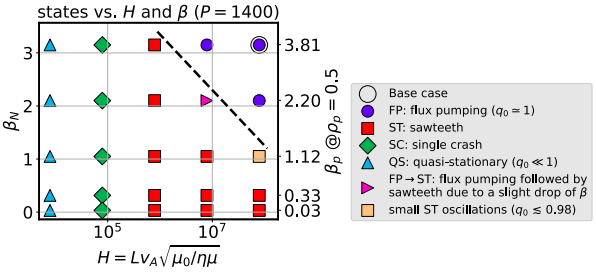

FIG. 9. Different plasma states at different Hartmann numbers and plasma betas. β_p is evaluated at half the minor radius. The dashed line roughly marks the boundary for accessing flux pumping. P is fixed at 1400 for all cases.

Flux pumping only exists at the upper-right corner of the β-H diagram, indicating the strict conditions for avoiding sawteeth (the β threshold and low enough system dissipation). Nevertheless, at the experimental dissipation ($H = 7.9 \times 10^7$), flux pumping is retained even at a lower $\beta_N \simeq 2$ ($\beta_p \simeq 2.2$) in the modeling, which differs from the experimental operating window (sawteeth were observed when $\beta_N \simeq 2$ in the AUG discharge #36663) [3]. Further lowering β leads to the transition from flux pumping to sawteeth at $\beta_N \simeq 1$ ($\beta_p \simeq 1.1$), as indicated by the yellow rectangle. In this state, the core plasma exhibits periodic oscillations resembling small sawteeth and q_0 is reduced slightly below 0.98 before each crash. However, if the dissipation level is increased by an order of magnitude ($H = 7.9 \times 10^6$), due to the increased stabilization effect on the mode, the boarder between flux pumping and sawteeth is obtained at $\beta_N \simeq 2$ ($\beta_p \simeq 2.2$, the pink right triangle), which is more comparable with the experimental observation to a certain extent. In this case, the core plasma first evolves into flux pumping and then transits into sawtoothing state due to a slight drop of β by several percent. Compared with the AUG experiments, the lower threshold of β at $H = 7.9 \times 10^7$ for accessing flux pumping in current JOREK modeling is attributed to the single-fluid physical basis used in these studies to limit computational costs. In contrast, the ongoing two-fluid modeling [14] and hybrid modeling (with kinetic EPs) [23] would be essential for precisely demonstrating the threshold of flux pumping, though these become increasingly challenging at low dissipations.

4. CONCLUSION AND DISCUSSION

In this work, the flux pumping discharge (#36663) of the AUG hybrid scenario has been systematically modeled based on the two-temperature, full MHD model of JOREK. The study commences with a comparison of 2D/3D nonlinear simulations at realistic parameters against the experimental observations. The simulation reproduces the radial redistribution of current density in the plasma center due to the continuous dynamo electric field generated by the 1/1 MHD mode. The dynamo of the order of mV/m is negative in the core and positive at $\rho_p \gtrsim 0.2$, which clamps the flat current density at the amplitude of 2.5 MA/m^2 and the central shear-free q profile around 1.0, thereby preventing sawtooth onset. The simulation results at AUG parameters are quantitatively consistent with the experimental observations in terms of current redistribution and dynamo electric field in the presence of flux pumping.

In this context, parameter scans have been performed to investigate plasma bifurcations at different system dissipations and plasma betas. By increasing the resistivity and viscosity, equivalent to decreasing the Hartmann number, four regimes of core plasma states are identified. First, flux pumping is obtained at extremely low dissipation ($H \gtrsim 10^7$, well beyond the typical range modeled for tokamak or RFP plasmas, i.e., $H \lesssim 10^5$). Secondly, sawtooth oscillations are observed at moderate dissipations ($10^5 \lesssim H \lesssim 10^7$). The intermittent dynamo electric field is responsible for raising the q_0 to unity during the core relaxation collapse. Thirdly, at the higher dissipation ($10^4 \lesssim H \lesssim 10^6$), the single giant sawtooth crash state followed by a quasi-stationary 1/1 resistive internal kink mode is observed. The later stage is similar to flux pumping with a continuous dynamo offsetting the current drive, during which q_0 (~ 0.9) is relatively lower than unity but much higher than that of the 2D case. The final state of the highest dissipation ($H \lesssim 10^4$) corresponds to the complete failure of the dynamo to sustain or modulate the q profile (the dynamo amplitude is at noise level). Therefore, q_0 directly decreases to the value (~ 0.7) close to the 2D case. The bifurcated plasma behaviours at different Hartmann numbers are qualitatively consistent with existing MHD modeling of FRP and tokamak plasmas, where the laminar QS/QSH state was obtained at high Hartmann number with helical boundary conditions [19, 20] and the quasi-stationary flux pumping state was found at a relatively low viscosity regime [16]. This work bridges the previous MHD modeling of sawtooth or similar plasma relaxation events at moderate Hartmann number [9, 15–21] and the latest quantitative simulation of flux pumping at experimentally relevant high Hartmann numbers [11]. Meanwhile, the plasma beta threshold for accessing flux pumping in full MHD modeling is evaluated. The result is qualitatively consistent with the AUG experiments, but also suggesting the necessity of improving the extended simulation model, in particular by including two-fluid effects [14], the kinetic EPs [23], and the relevant fishbones [3, 22].

In parallel, the studies involving the current source scan, the EP/fishbone effects, the modeling targeting JET flux pumping experiments [5, 7], and the extended MHD development are being conducted. These efforts are critical for understanding flux pumping through direct 3D MHD simulations and for calibrating the fast surrogate model being developed [24]. The surrogate model aims to efficiently predict the dynamo amplitude and assess the feasibility of flux pumping in existing tokamaks like AUG and JET, and future larger devices like ITER and DEMO.

ACKNOWLEDGEMENTS

The author H. Zhang would like to acknowledge D. Bonfiglio, E. Fable and F. Stefanelli for valuable discussions, and J. Stober for reviewing the manuscript and providing constructive suggestions. The simulations were finished mainly on the supercomputers (Marconi-Fusion, Leonardo, Pitagora) hosted by CINECA in Italy, the JFRS-1 supercomputer at IFERC-CSC in Japan, and the TOK cluster at the Max Planck Institute for Plasma Physics in Germany. This work has been carried out within the framework of the EUROfusion Consortium, funded by the European Union via the Euratom Research and Training Programme (Grant Agreement No 101052200 EUROfusion). Views and opinions expressed are however those of the author(s) only and do not necessarily reflect those of the European Union or the European Commission. Neither the European Union nor the European Commission can be held responsible for them.

REFERENCES

[1] I. Chapman, et al. Power requirements for electron cyclotron current drive and ion cyclotron resonance heating for sawtooth control in ITER. *Nuclear Fusion*, 53(6):066001, 2013.

[2] C. C. Petty, et al. Magnetic-Flux Pumping in High-Performance, Stationary Plasmas with Tearing Modes. *Physical Review Letters*, 102:045005, 2009.

[3] A. Burckhart, et al. Experimental evidence of magnetic flux pumping in ASDEX upgrade. *Nuclear Fusion*, 63(12):126056, 2023.

[4] W. Z. Mao, et al. Fluctuation-induced dynamo effect in a magnetic confinement plasma. *Physical Review Research*, 5:L022047, 2023.

[5] A. Burckhart, et al. Magnetic Flux Pumping at JET. In *50th EPS Conference on Plasma Physics*, 2024.

[6] W. Boyes, et al. Novel intrinsic helical cores and MHD dynamo flux pumping evidence in DIII-D. *Nuclear Fusion*, 64(12):124005, 2024.

[7] A. Bock, et al. Flux Pumping in ASDEX Upgrade, JET and JOREK. 2025. this conference.

[8] S. C. Jardin, et al. Self-Organized Stationary States of Tokamaks. *Physical Review Letters*, 115:215001, 2015.

[9] I. Krebs, et al. Magnetic flux pumping in 3D nonlinear magnetohydrodynamic simulations. *Physics of Plasmas*, 24(10):102511, 2017.

[10] Q. Yu, et al. Numerical modelling of sawteeth and sawtooth-free regime. *Nuclear Fusion*, 64(8):086053, 2024.

[11] H. Zhang, et al. Quantitative magnetohydrodynamic modelling of flux pumping in ASDEX Upgrade. *Nuclear Fusion*, 65(6):066001, 2025.

[12] R. E. Denton, et al. The m=1 convection cell and sawteeth in tokamaks. *The Physics of Fluids*, 30(5):1448–1451, 1987.

[13] F. D. Halpern, et al. Oscillation regimes of the internal kink mode in tokamak plasmas. *Plasma Physics and Controlled Fusion*, 53(1):015011, 2010.

[14] F. D. Halpern, et al. Diamagnetic thresholds for sawtooth cycling in tokamak plasmas. *Physics of Plasmas*, 18(10):102501, 2011.

[15] W. Shen, et al. Linear and nonlinear simulations of the visco-resistive internal kink mode using the M3D code. *Nuclear Fusion*, 58(10):106035, 2018.

[16] W. Zhang, et al. Sawtooth relaxation oscillations, nonlinear helical flows and steady-state m/n=1 magnetic islands in low-viscosity tokamak plasma simulations. *Nuclear Fusion*, 60(9):096013, 2020.

[17] S. Cappello, et al. Bifurcation in Viscoresistive MHD: The Hartmann Number and the Reversed Field Pinch. *Physical Review Letters*, 85:3838–3841, 2000.

[18] S. Cappello, et al. Magnetohydrodynamic dynamo in reversed field pinch plasmas: Electrostatic drift nature of the dynamo velocity fielda). *Physics of Plasmas*, 13(5):056102, 2006.

[19] D. Bonfiglio, et al. Experimental-like Helical Self-Organization in Reversed-Field Pinch Modeling. *Physical Review Letters*, 111:085002, 2013.

[20] M. Veranda, et al. Helically self-organized pinches: dynamical regimes and magnetic chaos healing. *Nuclear Fusion*, 60(1):016007, 2019.

[21] P. Piovesan, et al. Role of a continuous MHD dynamo in the formation of 3D equilibria in fusion plasmas. *Nuclear Fusion*, 57(7):076014, 2017.

[22] S. Günter, et al. The influence of fishbones on the background plasma. *Nuclear Fusion*, 39(11):1535, 1999.

[23] Y. I. Kolesnichenko, et al. Stabilization of the quasi-interchange mode in tokamaks by circulating energetic ions. *Physics of Plasmas*, 14(1):012504, 2007.

[24] I. Krebs, et al. Reduced model of magneto-hydrodynamic dynamo enabled magnetic flux pumping for scenario development of hybrid tokamak discharges. In *49th EPS Conference on Plasma Physics*, 2023.